

Variational Multiscale Element Free Galerkin Method for Three-dimensional Steady Convection-Diffusion Problems

Xiaoting Cao, Xiaohua Zhang*

Abstract—The variational multiscale element free Galerkin method (VMEFG) is extended to address three-dimensional(3D) steady-state convection-dominated problems. The scheme is composed by developing the element free Galerkin method to the 3D aspect and combined with the variational multiscale method. In this work, the fine-scale solutions enable to be acquired by bubble functions and then substituted into the coarse-scale part to further find the coarse-scale solution. The stability term is naturally determined in this process. Furthermore, the arbitrary convex polygonal influence domain technique is promoted to have an arbitrary convex polyhedral influence domain, thus increasing the computing efficiency and simplifying the algorithm. Meanwhile, the dimensionless size is set to 1.01 for the influence domain, which makes the shape function interpolative and explains the direct imposition of the essential boundary conditions. For validating the efficiency of this proposed method, four 3D steady convection-diffusion equations are calculated, and the numerical solutions are considered for comparison with those of the EFG method. The results demonstrate that the VMEFG method can achieve higher computational precision than the EFG method. Moreover, the present method can virtually eliminate the nonphysical oscillations that arise in the EFG method while addressing the convection-dominated problems.

Index Terms—element free Galerkin method, variational multiscale method, convection-dominated, bubble functions, 3D steady convection-diffusion.

I. INTRODUCTION

THE convection-diffusion equation is considered one of the most widely used models, which involves various engineering fields such as fluid dynamics and environmental science. However, accurately finding the numerical solution of convection-diffusion problems has become a challenging study in computational mechanics. Yet, there are the main numerical methods for solving convection-diffusion problems that can be viewed in the literature [1]–[3]. Nonetheless, these methods highly rely on the mesh quality and suffer from difficulties in meshing complex domains. On account of these deficiencies, various numerical methods, namely the meshless method, have been well developed to avoid the above-mentioned deficiencies in recent years, which have achieved significant success in calculating partial differential equations. The most attractive feature of the meshless method

is that it does not rely on the mesh and only demands a group of nodes distributed on the problem domain and its boundaries.

Numerous meshless methods have been proposed so far. More details on the categorization, application, and computer implementation for meshless methods can be referenced in some literature [4]–[7]. From these studies, it can be observed that the element-free Galerkin method (EFG) serves as a vital meshless method. It approximates the shape function using the moving least squares method (MLS) [8], [9], allowing continuous functions with higher-order derivatives to be easily constructed even using a linear basis and ensuring that the second-order derivative term in the stabilization term is not neglected. Consequently, the EFG method guarantees calculational accuracy and numerical stability. The algorithm is quite simple, which has been proven to be a powerful numerical method for discussing a series of physical and engineering problems. For the strong convection-dominated diffusion problem, it is difficult to simulate in mechanics and mathematics because of its strongly hyperbolic nature [10]. Nevertheless, the conventional meshless method based on Galerkin weak forms can not numerically solve the strong convection-dominated problem since it usually leads to unphysical oscillations in the boundary or interior layers.

Over several decades, researchers have proposed a wide range of stabilized methods to avoid spurious numerical oscillations, which was presented in [11]. Combining these methods with meshless methods has generated a series of so-called stable meshless methods for dealing with convection-diffusion problems. For example, Wu et al. [12] introduced the SUPG scheme to eliminate over and under-shoots generated by the convection term in the Meshless Local Petrov-Galerkin method (MLPG). Chen et al. [13] proposed a new definition of the stability parameter in the Streamline Upwind Meshless Petrov-Galerkin method (SUMPLPG) to solve 2D convection-diffusion problems with large Peclet numbers. To the best of our knowledge, various other stable meshless approaches have been introduced and applied to approximate the solution of the convection-diffusion equation numerically. A brief overview can be given below. The meshless method, in combination with the Reproducing Kernel Particle Method (RKPM), was adopted as an efficient approach towards the 2D advection-diffusion problem. Romão [15] numerically solved the 3D convection-diffusion-reaction equations by using Galerkin and least-square FEM. Cheng et al. [16] presented the hybrid improved complex variable element-free Galerkin method (H-ICVEFG) for 3D unstable state advection-diffusion problems. Ma et al. [17] developed the dimension splitting element-free Galerkin method (DSEFG)

Manuscript received October 4, 2021; revised March 3, 2022. This work is financially supported by the National Natural Science Foundation of China (No. 11972216).

Xiaoting Cao is a postgraduate student of the College of Science, China Three Gorges University, Yichang 443002, China (e-mail: caoxiaoting22@163.com).

*Xiaohua Zhang is an associate professor of the Three Gorges Mathematical Research Center, China Three Gorges University, Yichang 443002, China (corresponding author to provide phone: +8615872481386; e-mail: zhangxiaohua07@163.com).

to solve 3D advection-diffusion problems.

Although these works have achieved accurate and stable numerical solutions, a significant drawback is that the stability parameter [18] is often defined by the given problem and applied algorithm. Stated differently, whereas these methods can perform the function of diminishing the spurious oscillations, no valid algorithm is actually available to construct stable parameters or functions intimately associated with the stability and precision of the numerical method. Recently, Zhang [19] incorporated the variational multiscale method (VMS) in the EFG method, thus proposing the variational multiscale element free Galerkin method (VMEFG). Hence, the VMEFG method can fully utilize the benefits of the above two methods. An important inherited feature of the present method is that no user-defined stabilization parameters are required. This method has successfully addressed diverse engineering issues, and please consult these papers [20]–[24] for details. Until now, some researchers have developed a few methods on the basis of the VMEFG method. For instance, by converting the shape function approximation method from the MLS to be the interpolating moving least squares method (IMLS), Zhang and Li [25] presented a variational multiscale interpolating element free Galerkin method (VMIEFG) for 2D convection-diffusion and Stokes problems. Wang and Sun [26] developed a hybrid VMEFG method by coupling the dimension splitting method with the VMEFG method for 2D convection-diffusion problems. Recently, the VMEFG method has also been studied and extended by several researchers abroad. For example, Dehghan et al. [27] use the VMEFG method with the moving Kriging interpolation for discontinuous problems. Peddavarapu and Raghuraman [28] proposed the Maximum entropy-based variational multiscale element free Galerkin method by adopting first-order local maximum entropy (LME) basis functions for scalar 2D advection-diffusion problems.

Nevertheless, no published results are available for VMEFG methods for 3D stable convection-diffusion problems. Even up to date, there are few studies on meshless methods for 3D convection-diffusion problems. Investigating its reasons are mainly twofold: one is that numerical calculations of 3D problems often tend to be more complicated and computationally intensive, while the other is that other methods still encounter difficulties in determining stability parameters straightforward. And yet, the VMEFG method can overcome these issues. Consequently, investigating the VMEFG method for 3D convective-diffusion problems is of great research value.

In this article, we apply the VMEFG method to solve the 3D steady convection-diffusion problem. We have done the work as follows. First, we obtain the fine-scale solution using the bubble function and substitute it into the coarse-scale to accept the coarse-scale solution numerically. The the process naturally determines the stability term. Then, we expand the nodal influence domain technique for the convex polygon to the nodal influence domain of arbitrary convex polyhedron. This technique allows avoiding the node search process greatly and significantly reducing the bandwidth of the global stiffness matrix, thus improving the computational efficiency of the proposed method. In the end, letting the influence factor of the nodal influence domain equal to 1.01 enables the shape function to satisfy the properties of the

Kronecker Delta condition so that it can directly impose the essential boundary condition, leading to a considerable improvement in the computing efficiency of the present method.

The remainder of the paper is outlined as follows. In Section II, the moving least squares (MLS) approximation method and the extension of the arbitrary convex polygonal influence domain technique are proposed. In Section III, the derivation of the VMEFG method for solving the 3D convection-diffusion equation is expressed. Four numerical examples are presented to illustrate the effectiveness and accuracy of the present method, and analysis is performed in Section IV. Some conclusions and future studies are drawn in Section V.

II. THE MLS APPROXIMATION AND THE EXTENSION OF THE ARBITRARY CONVEX POLYGONAL INFLUENCE DOMAIN TECHNIQUE

A. The MLS approximation

The MLS method is widely used to construct meshless shape functions. The MLS approximation function for the unknown function $U(\mathbf{x})$ over the domain Ω is defined as [29]

$$U^h(\mathbf{x}) = \sum_{j=1}^m \phi_j(\mathbf{x})\mu_j(\mathbf{x}) = \phi^T(\mathbf{x})\boldsymbol{\mu}(\mathbf{x}), \quad (1)$$

where $\phi(\mathbf{x})$ is a complete polynomial basis function vector with the number m , and $\mathbf{x} = [x, y, z]^T$ is the 3D space coordinate, while $\boldsymbol{\mu}(\mathbf{x}) = [\mu_1(\mathbf{x}), \mu_2(\mathbf{x}), \dots, \mu_m(\mathbf{x})]^T$ is coefficient vector needed to be sorted out. In three dimensions, the linear basis function is chosen and can be written as follows

$$\phi^T(\mathbf{x}) = (1, x, y, z). \quad (2)$$

The unknown coefficient $\boldsymbol{\mu}(\mathbf{x})$ in Eq.(1) can be found via minimizing the weighted discrete L_2 error norm below

$$J = \sum_{i=1}^n w(\mathbf{x} - \mathbf{x}_i)[U_i - \phi^T(\mathbf{x}_i)\boldsymbol{\mu}(\mathbf{x})]^2, \quad (3)$$

where n refers to the number of nodes that contain points \mathbf{x} in the nodal support domain, $w(\mathbf{x} - \mathbf{x}_i)$ indicates a weight function of the influence domain of node \mathbf{x}_i , U_i is the node value of the function U at node $\mathbf{x} = \mathbf{x}_i$.

According to the minimization condition of Eq.(3), the resulted system of linear equations with respect to the coefficient $\boldsymbol{\mu}(\mathbf{x})$ can be obtained as follows

$$\mathbf{A}(\mathbf{x})\boldsymbol{\mu}(\mathbf{x}) = \mathbf{B}(\mathbf{x})U, \quad (4)$$

in which

$$\mathbf{A}(\mathbf{x}) = \sum_{i=1}^n w_i(\mathbf{x})\phi(\mathbf{x}_i)\phi^T(\mathbf{x}_i), \quad (5)$$

$$\mathbf{B}(\mathbf{x}) = [w_1(\mathbf{x})\phi(\mathbf{x}_1), w_2(\mathbf{x})\phi(\mathbf{x}_2), \dots, w_n(\mathbf{x})\phi(\mathbf{x}_n)], \quad (6)$$

$$w_i(\mathbf{x}) = w(\mathbf{x} - \mathbf{x}_i). \quad (7)$$

The vector $\boldsymbol{\mu}(\mathbf{x})$ can be given as follows in the case that \mathbf{A} is invertible.

$$\boldsymbol{\mu}(\mathbf{x}) = \mathbf{A}^{-1}(\mathbf{x})\mathbf{B}(\mathbf{x})U. \quad (8)$$

Eq.(8) is substituted into Eq.(1) to yield

$$U^h(\mathbf{x}) = \phi^T(\mathbf{x})\mathbf{A}^{-1}(\mathbf{x})\mathbf{B}(\mathbf{x})\mathbf{U} = \mathcal{N}^T(\mathbf{x})\mathbf{U}, \quad (9)$$

in which the definition of the shape function is presented by

$$\mathcal{N}^T(\mathbf{x}) = \phi^T(\mathbf{x})\mathbf{A}^{-1}(\mathbf{x})\mathbf{B}(\mathbf{x}). \quad (10)$$

Generally, the shape functions gained by MLS fail to meet the Kronecker Delta conditional property at each node. This means that the boundary conditions are impossible to enable straightforward imposition. Nowadays, several techniques have been proposed for this problem. For instance, the Lagrange multiplier method and penalty method [30], etc. Actually, these techniques may have the disadvantage of increasing the complexity of solving the problem and requiring more computational time. In this article, a brief technique is employed to extend the nodal influence domain of the cubic or spherical shape to arbitrary convex polyhedral shapes, as described with more details in the next section II-B.

B. Weight functions and the extension of the arbitrary convex polygonal influence domain technique

The weight function can be arbitrarily chosen, while the spline function has been broadly utilized in numerical experiments. In this article, we choose the cubic spline function, defined as follows

$$w_i(\mathbf{x} - \mathbf{x}_i) = w(q) = \begin{cases} \frac{2}{3} - 4q^2 + 4q^3, & q \leq \frac{1}{2}, \\ \frac{4}{3} - 4q + 4q^2 - \frac{4}{3}q^3, & \frac{1}{2} \leq q \leq 1, \\ 0, & q \geq 1, \end{cases} \quad (11)$$

where $q = \frac{\|\mathbf{x} - \mathbf{x}_i\|}{r_i}$, $\|\mathbf{x} - \mathbf{x}_i\|$ indicates the distance from point \mathbf{x} to node \mathbf{x}_i , and $r_i = \alpha\rho_i$ represents the influence radius of node \mathbf{x}_i , in which α and ρ_i denote the dimensionless size of the influence domain and the distance between two adjacent nodes, respectively. For 3D problems, the cube or sphere is generally employed to be the nodal influence domain. As for nodal influence domain with the cubic shape, its weight function is determined as

$$w_i(\mathbf{x}) = w(q_x)w(q_y)w(q_z), \quad (12)$$

where $q_x = \frac{|x-x_i|}{r_x}$, $q_y = \frac{|y-y_i|}{r_y}$, $q_z = \frac{|z-z_i|}{r_z}$, r_x, r_y, r_z express the radius of the influence domain along x-axis, y-axis, and z-axis respectively.

The nodal influence domain size significantly impacts the computational accuracy of the points. Recently, Zhang et al. [31] proposed the arbitrary convex polygonal influence domain technique adopted for 2D problems. In this technique, the influence domain of rectangular or circular nodes of the meshless method is expanded to any arbitrary polygon, which provides high computational accuracy and considerably improves the computing efficiency of the meshless method. Considering these advantages, an extension of this technique to 3D problems is presented in this paper.

In 3D space, the general influence domain is expanded to arbitrary convex polyhedral shapes consisting of tetrahedrons. In this setting, when the dimensionless size of the influence domain is close to 1, the Gauss points in each

tetrahedral background cell have only devoted the nodes in that tetrahedron. Thus, the node search procedure can be greatly avoided, and the bandwidth of the global stiffness matrix is significantly reduced [32]. Besides, the shape function is almost interpolative, leading that the essential boundary conditions can still be dealt with directly. Overall, the extended techniques can improve computational efficiency and simplify the imposition of essential boundary conditions.

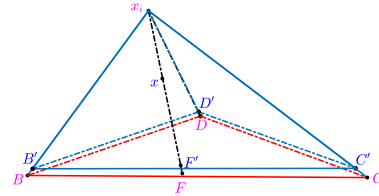


Fig. 1: A tetrahedron cell in the convex polyhedron influence domain of node \mathbf{x}_i

Taking a tetrahedron from the influence domain into consideration (see Fig.1), we give a conclusion of the procedure on how to compute the MLS shape function of node \mathbf{x}_i at point \mathbf{x} , where \mathbf{x} generally represents the Gauss point.

- (1) Identify the tetrahedron where point \mathbf{x} belongs;
 - (2) Find point F' in which the line $\mathbf{x}_i\mathbf{x}$ intersects the plane $B'C'D'$. The analytical expressions of the line can be obtained by the node \mathbf{x}_i and point \mathbf{x} , and the plane can be determined by nodes B', C', D' in the tetrahedron cell, which can easily get the intersection point by combining the two analytical expressions;
 - (3) Determine the length of \mathbf{x}_iF' with the two-point distance formulation;
 - (4) Employ the formula $\mathbf{x}_iF = \alpha\mathbf{x}_iF'$;
 - (5) The influence radius $r_i = \mathbf{x}_iF$ along the $\overrightarrow{\mathbf{x}_i\mathbf{x}}$ direction can be derived;
 - (6) As soon as the influence radius r_i and q are determined, it is convenient to gain the weight function via Eq.(11). Then, the shape function can be further determined by Eq.(12).
- In this paper, we let $\alpha = 1.01$. At this moment, this technique possesses the above benefits.

III. THE VMEFG METHOD FOR CONVECTION-DIFFUSION EQUATION

A. The standard weak form

In this paper, 3D steady convection-diffusion equation is considered, which is given by the following equation with the definition over the cubic domain Ω

$$\mathbf{c} \cdot \nabla - k\Delta U = f, \quad \text{in } \Omega, \quad (13)$$

$$U = \psi, \quad \text{on } \Gamma, \quad (14)$$

where $\mathbf{c} = (c_x, c_y, c_z)^T$, c_x, c_y, c_z refer to the convective coefficient along x-axis, y-axis and z-axis respectively, coefficient $k \geq 0$ denotes the diffusivity, f and ψ represent a known source term and the boundary condition.

Let $V \subset H^1(\Omega) \cap C^0(\Omega)$ represent the space of trial functions for the unknown scalar field, then the variational

form corresponding to Eq.(13) is to find $U \in W = H_0^1(\Omega)$ satisfying

$$(w, \mathbf{c} \cdot \nabla U) + (\nabla w, k \nabla U) = (w, f), \quad \forall w \in V, \quad (15)$$

where w denotes the weighting function for U , and $(\cdot, \cdot) = \int_{\Omega} (\cdot) d\Omega$ is the inner product in $L_2(\Omega)$.

B. The VMEFG method

The VMEFG method is extended to derive a stable formulation for the 3D steady convection-diffusion equation. The main idea is splitting the scalar field and weight function into coarse and fine scales. Then they are substituted into the standard variational form. Thus, the problem can be divided into coarse and fine-scale parts. Applying bubbles to express the fine-scale can further yield the fine-scale solution. By substituting the solution back into the coarse-scale part, we can get the coarse-scale solution. In eliminating the fine scales, the stability term is determined naturally. Assume that the test function U and the weighting function w are respectively divided into coarse and fine scales, denoted as

$$U = \bar{U} + U', w = \bar{w} + w'. \quad (16)$$

As for 3D convection-diffusion problems, the derivation process of the fine-scale and coarse-scale solutions approximates that in 2D. So many details can be referred to in the articles [32], [33]. Only the final weak form is presented below

$$\begin{aligned} & (\bar{w}, \mathbf{c} \cdot \nabla \bar{U}) + (\nabla \bar{w}, k \nabla \bar{U}) \\ & + (\mathbf{c} \cdot \nabla \bar{w} + k \Delta \bar{w}, \tau (\mathbf{c} \cdot \nabla \bar{U} - k \Delta \bar{U})) \quad (17) \\ & = (\bar{w}, f) + (\mathbf{c} \cdot \nabla \bar{w} + k \Delta \bar{w}, \tau f), \end{aligned}$$

where $\bar{U}(x)$ and $U'(x)$ represent trial function respectively in coarse-scale and fine-scale, whereas $\bar{w}(x)$ and $w'(x)$ are weighting solutions respectively in coarse-scale and fine-scale. τ is designated as the stability parameter given as the following:

$$\tau = \frac{b_1^{cell} \int_{\Omega^{cell}} b_2^{cell} d\Omega}{(b_2^{cell}, \mathbf{c} \cdot \nabla b_1^{cell}) + (\nabla b_2^{cell}, k \nabla b_1^{cell})}, \quad (18)$$

in which b_1^{cell} and b_2^{cell} indicate the bubble functions for the trial solutions and weighting functions, correspondingly. It is worth noting that the bubble functions make the present 3D problems different from 2D problems. The bubble function is concisely introduced in the next Section III-C.

Eq.(17) represents the ultimate variational multiscale form, and we compare it with the standard variational form. Note that the third term at the left and second term at the right in this equation expresses additional stability terms, which preserve the fine-scale effects. Furthermore, the stabilization parameter emerged spontaneously from addressing the fine-scale problem.

The stable form Eq.(17) is eventually represented in coarse scale for this problem. For keeping the representation simple, we dropped the superimposed bars and identified the final VMEFG form as

$$\begin{aligned} & (w, \mathbf{c} \cdot \nabla U) + (\nabla w, k \nabla U) \\ & + (\mathbf{c} \cdot \nabla w + k \Delta w, \tau (\mathbf{c} \cdot \nabla U - k \Delta U)) \quad (19) \\ & = (w, f) + (\mathbf{c} \cdot \nabla w + k \Delta w, \tau f). \end{aligned}$$

Associating Eq.(9) and Eq.(19) leads to the linear system of equation as below

$$(\mathbf{M} + \mathbf{K})\mathbf{U} = \mathbf{S}_1 + \mathbf{S}_2, \quad (20)$$

where $\mathbf{U} = [U_1, U_2, \dots, U_n]$, and

$$[\mathbf{M}]_{ij} = \int_{\Omega} \mathcal{N}_i (\mathbf{c} \cdot \nabla \mathcal{N}_j) d\Omega + \int_{\Omega} \nabla \mathcal{N}_i \cdot k \nabla \mathcal{N}_j d\Omega,$$

$$[\mathbf{K}]_{ij} = \int_{\Omega} (\mathbf{c} \cdot \nabla \mathcal{N}_i + k \Delta \mathcal{N}_i) \cdot \tau \cdot (\mathbf{c} \cdot \nabla \mathcal{N}_j - k \Delta \mathcal{N}_j) d\Omega,$$

$$[\mathbf{S}_1]_i = \int_{\Omega} \mathcal{N}_i f d\Omega,$$

$$[\mathbf{S}_2]_i = \int_{\Omega} (\mathbf{c} \cdot \nabla \mathcal{N}_i + k \Delta \mathcal{N}_i) \tau f d\Omega.$$

C. Bubble functions

An appropriate bubble function b^{cell} needs to meet the following properties.

$$b^{cell} > 0, \quad \forall \mathbf{x} \in \Omega^{cell};$$

$$b^{cell} = 0, \quad \forall \mathbf{x} \in \partial \Omega^{cell};$$

$$\exists \mathbf{x} \in \Omega^{cell} \text{ s.t. } b^{cell}(\mathbf{x}) = 1.$$

In 3D case, the internal point that satisfies $b^{cell} = 1$, which is denoted by the point $(\frac{1}{4}, \frac{1}{4}, \frac{1}{4})$ of the unit reference tetrahedron in this paper, and the bubble for the trial solution in fine scale is defined as

$$b_1^{cell}(x, y, z) = 256xyz(1 - x - y - z). \quad (21)$$

Concerning the weighting function in fine scale, the unit

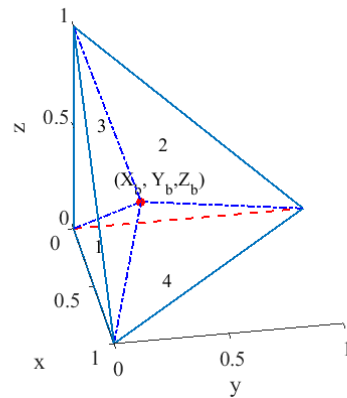


Fig. 2: The bubble function representing the fine-scale weighting function on a unit referenced tetrahedron

reference tetrahedron is partitioned into four regions, as depicted in Fig.2. The definition of the bubble functions on these regions are given as follows

$$b_2^{cell}(x, y, z) = \begin{cases} \frac{xyz}{X_b Y_b Z_b}, & \text{for } x, y, z \text{ in region } 1, 3, 4, \\ \frac{1-x-y-z}{1-X_b-Y_b-Z_b}, & \text{for } x, y, z \text{ in region } 2, \end{cases} \quad (22)$$

where X_b , Y_b and Z_b indicate the position of the internal virtual node in the background cell.

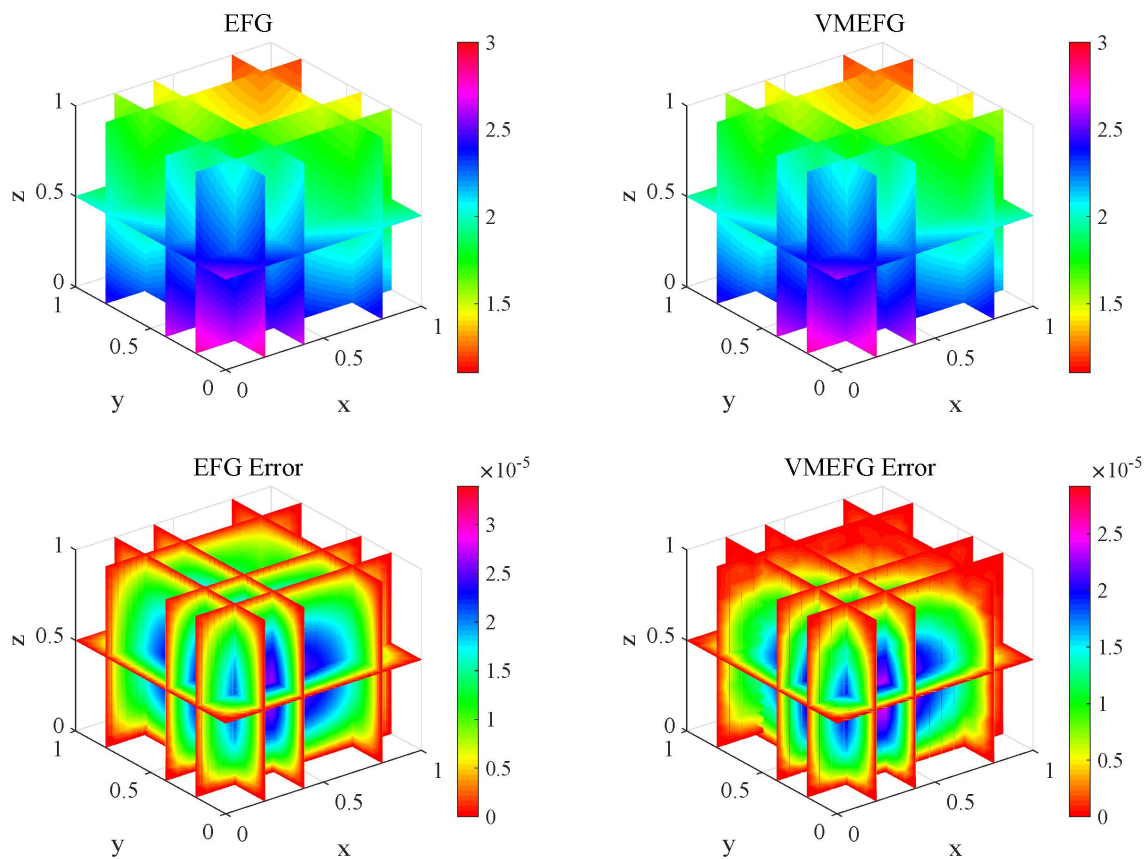


Fig. 3: The elevation plots of solutions for Case 1 with 16^3 nodes (a) EFG solution (top,left); (b) VMEFG solution (top,right); (c) EFG absolute error (bottom,left); (d) VMEFG absolute error (bottom,right).

IV. NUMERICAL EXAMPLE

In this section, for illustrating that the present method has the capabilities in diminishing spurious oscillations near various layers with its stabilizing features against 3D steady convection-dominated diffusion problems, there are four 3D steady convection-diffusion problems with the variable coefficients to be solved that all have available analytical solution of their own respectively.

For all the test problems, $4 \times 4 \times 4$, $8 \times 8 \times 8$, $16 \times 16 \times 16$, $32 \times 32 \times 32$ nodes are distributed uniformly in hexahedral computational domain $[0, 1]^3$ and 384, 3072, 24576, 196608 tetrahedron background cells for the use of numerical integration, respectively. We consider 16 points of Gauss quadrature on each tetrahedral background integration cell to perform the integration throughout this section. Simultaneously compared with the conventional meshless method EFG to demonstrate the more validation of the VMEFG method in addressing the convection-dominated diffusion problem. In addition, the L_2 error norm is defined as

$$\|U^{num} - U^{exact}\|_{L_2} = \left(\int_{\Omega} (U_i^{num} - U_i^{exact})^2 d\Omega \right)^{1/2}.$$

Besides the L_2 error norm, the L_{∞} error norm defined as follows

$$\|U^{num} - U^{exact}\|_{L_{\infty}} = \max_{1 \leq i \leq n} |U_i^{num} - U_i^{exact}|.$$

The above approach proves that the present method can avoid numerical oscillations in the EFG method and obtain more precise solutions. In conclusion, the VMEFG method seems more applicable and precise than the EFG method

for this convection-dominated problem.

Example 1. For the first example, we consider the 3D steady convection-diffusion problem over the spatial domain $\Omega = [0, 1]^3$ with Dirichlet boundary conditions is taken into account, and the governing equation is as follows

$$\frac{1}{A} \frac{\partial^2 U}{\partial x^2} + \frac{1}{A} \frac{\partial^2 U}{\partial y^2} + \frac{1}{A} \frac{\partial^2 U}{\partial z^2} + \frac{\partial U}{\partial x} + \frac{\partial U}{\partial y} + \frac{\partial U}{\partial z} = 0.$$

This problem possesses the following analytical solution that is available in reference [15].

$$U(x, y, z) = e^{-x} + e^{-y} + e^{-z}.$$

Case 1 : We consider the value of $A = 1$. Fig.3 depicts the numerical solutions acquired by the EFG and VMEFG methods from a grid of 16^3 nodes in Case 1. From Figs.3(a) and 3(b), it seems clear that the two methods are adequately similar to each other in their results. Comparing Figs.3(c) with 3(d), we can easily find that the absolute errors of the VMEFG method are smaller as compared to that of the EFG method.

For further analysis, we extract the solution in the $z = 0.5$ plane from the above numerical solution. Then we can depict the numerical solution in the xy plane with $z = 0.5$, as depicted in Fig.4. As can be clearly observed, the difference between the two methods in the numerical solution is very small. But it is crucial to note that the VMEFG method leads to a more accurate solution than the EFG method.

Table I shows the L_2 error norm of the EFG and VMEFG methods. From this table, it can be directly seen that the

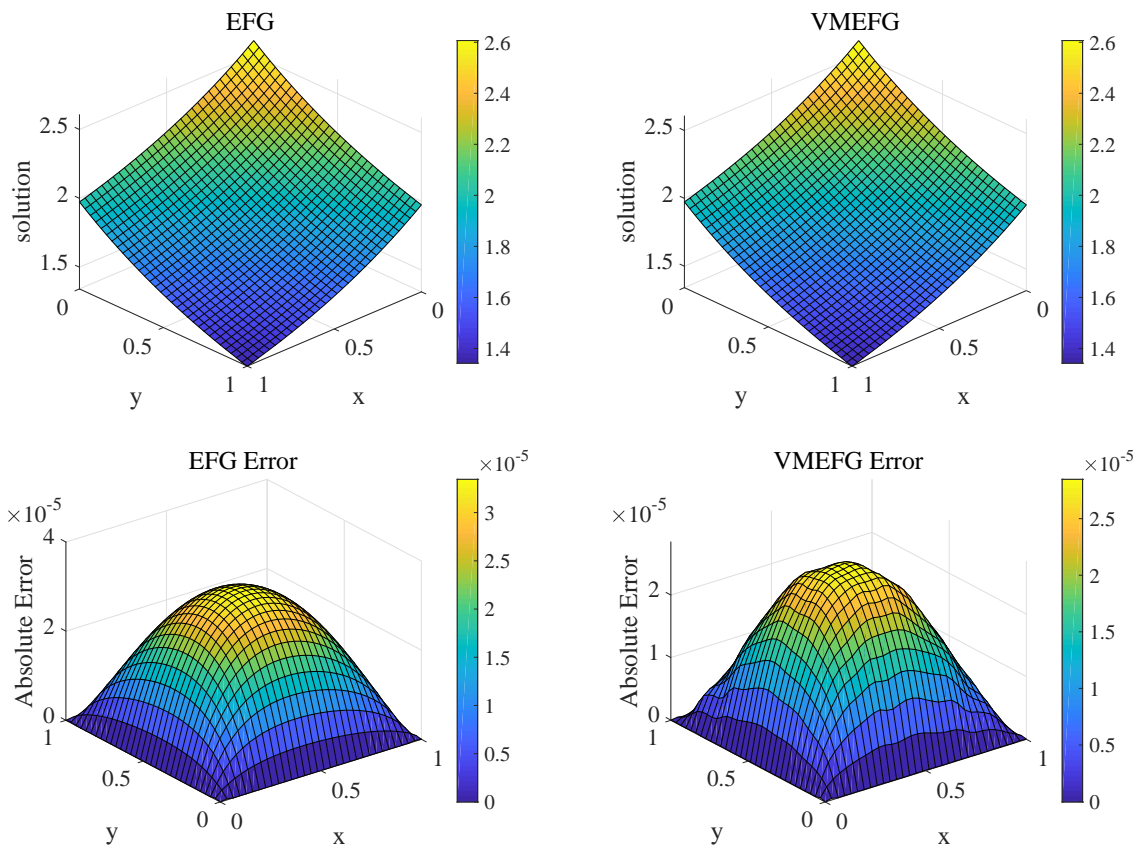


Fig. 4: The elevation plots of solutions for Case 1 with 16^3 nodes in plane $z = 0.5$ (a) EFG solution (top,left); (b) VMEFG solution (top,right); (c) EFG absolute error (bottom,left); (d) VMEFG absolute error (bottom,right).

TABLE I: Comparison of the L_2 error norms and convergence rates for Case 1

Number of nodes	h	EFG	rate	VMEFG	rate
125	1/4	1.540e-04		1.340e-04	
729	1/8	4.903e-05	1.651	4.271e-05	1.649
4913	1/16	1.360e-05	1.850	1.186e-05	1.849
35937	1/32	3.581e-06	1.925	3.124e-06	1.924

two methods both have pretty small L_2 error norms, but the VMEFG method has a smaller error norm than the EFG method under the same nodal distribution. Table I also lists the convergence rate of these two methods. From this table, the convergence rate of the VMEFG is nearly the same as the EFG under the same circumstance and approximate to 2. Generally speaking, the EFG and the VMEFG methods are both stable when solving the ordinary convection-diffusion problem.

In summary, the above comparison confirms that both the EFG and the VMEFG method achieve approximately two order accuracy, whereas the present VMEFG method achieves a more accurate solution. Relatively, the stability and effectiveness of these two methods are basically equivalent for the convection-diffusion problems in the general case.

Case 2 : We consider the value of $A = 1000$. In this setting, the convection coefficients are 1000 times larger than the diffusion coefficients, leading to a dominant convection problem. Fig.5 explicitly describes the computational solutions and absolute errors of the two methods obtained by

using 16^3 nodes. As shown apparently in Figs.5(a) and 5(c), we can observe that the EFG solution is discontinuous with large absolute errors. From Figs.5(b) and 5(d), it can be noted that the VMEFG solution is smooth, and its absolute error is relatively small, which ensures the stability and accuracy of its calculation. In comparison, the VMEFG method is higher stable and more accurate than the EFG method.

Furthermore, the numerical results in the xy plane with $z = 0.5$ are depicted in Fig.6. As we can see intuitively presented in Figs.6(a) and 6(c), the EFG solution varies sufficiently with apparent oscillations, and the absolute error is extremely large. In contrast with the EFG method, the VMEFG solution is almost coincident with the exact solution, and its absolute error is relatively small, as shown in Figs.6(b) and 6(d).

The above comparison confirms that the present VMEFG method can avoid the oscillations that appeared in the EFG method and obtain more precise solutions. In summary, the VMEFG method is more available and precise when compared with the EFG method for this convection-dominated problem.

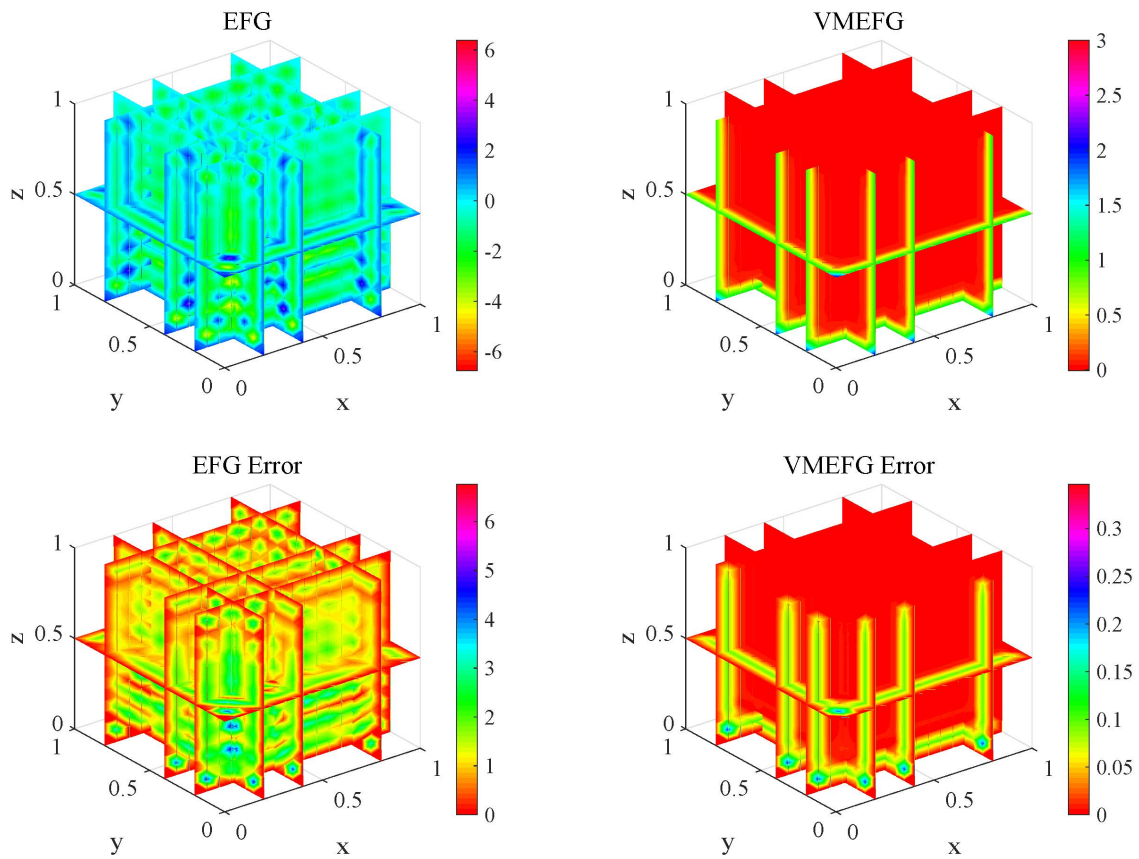


Fig. 5: The elevation plots of solutions for Case 2 with 16^3 nodes (a) EFG solution (top,left); (b) VMEFG solution (top,right); (c) EFG absolute error (bottom,left); (d) VMEFG absolute error (bottom,right).

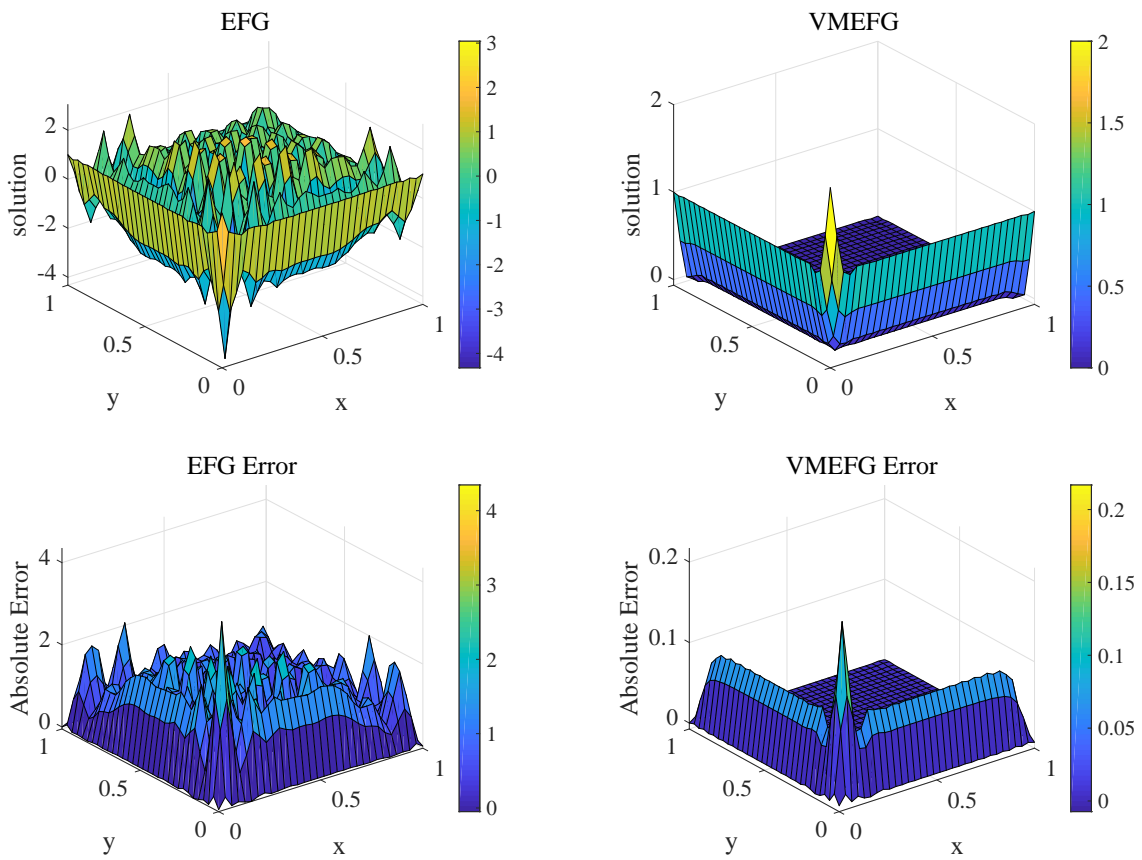


Fig. 6: The elevation plots of solutions for Case 2 with 16^3 nodes in plane $z = 0.5$ (a) EFG solution (top,left); (b) VMEFG solution (top,right); (c) EFG absolute error (bottom,left); (d) VMEFG absolute error (bottom,right).

TABLE II: Comparison of the L_2 and L_∞ norms of the error at $k = 10^{-3}$ for Example 2

Number of nodes	EFG			VMEFG		
	h	L_2 norm	L_∞ norm	h	L_2 norm	L_∞ norm
125	1/4	4.16e+00	1.98e+02	1/4	1.01e-01	4.60e-01
729	1/8	1.82e-01	1.02e+00	1/8	4.68e-02	1.32e-01
4913	1/16	1.14e+01	6.02e+01	1/16	1.60e-02	4.48e-02
35937	1/32	5.04e-03	1.66e-02	1/32	4.45e-03	1.21e-02

TABLE III: Comparison of the L_2 and L_∞ norms of the error at $k = 10^{-6}$ for Example 2

Number of nodes	EFG			VMEFG		
	h	L_2 norm	L_∞ norm	h	L_2 norm	L_∞ norm
125	1/4	4.15e+03	1.96e+04	1/4	8.91e-02	4.41e-01
729	1/8	1.53e+02	7.31e+02	1/8	3.64e-02	1.39e-01
4913	1/16	2.43e-02	1.10e-01	1/16	1.14e-02	3.06e-02
35937	1/32	7.91e-01	4.15e+00	1/32	3.73e-03	1.04e-02

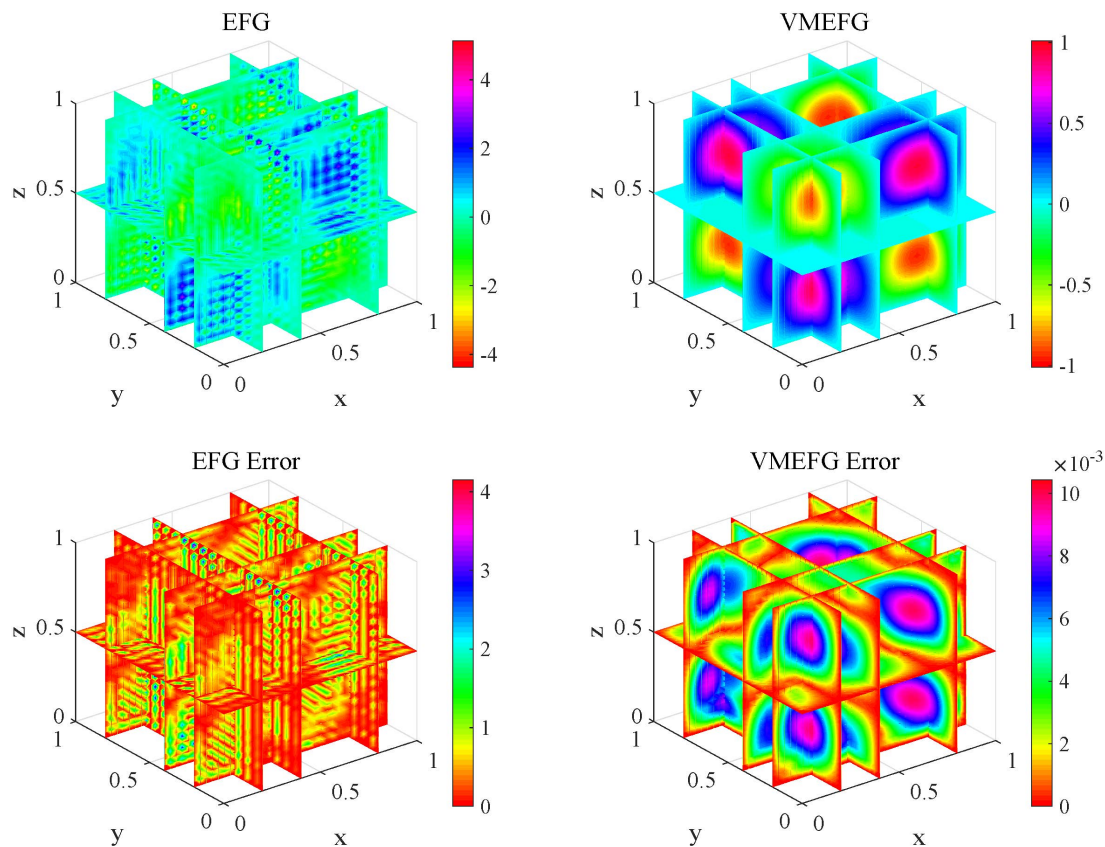


Fig. 7: The elevation plots of solutions for Example 2 with 32^3 nodes (a) EFG solution (top,left); (b) VMEFG solution (top,right); (c) EFG absolute error (bottom,left); (d) VMEFG absolute error (bottom,right).

Example2. This example considers the following differential equation with small diffusion velocity $k = 10^{-3}$ and $k = 10^{-6}$, $c = [1, 2, 1]^T$. The choice of f allows the exact solution to be given as follows, which can be found in reference [35]

$$U(x, y, z) = \sin(2\pi x)\sin(2\pi y)\sin(2\pi z).$$

The results are listed in Table II and Table III, which shows the L_2 norm and L_∞ norm of the error when $k = 10^{-3}$ and $k = 10^{-6}$. For the two cases, with the step size refining

gradually, the error of the two methods both decreased. But in any case, the error of the VMEFG method is always lower in contrast to the EFG method under the same conditions. In the convection-dominated case of $k = 10^{-3}$, it can be obtained from Table II that the VMEFG method has the accurate computed solution, while the EFG method also can get a satisfactory numerical solution with the step size refinement.

In the highly convection-dominated case of $k = 10^{-6}$, the L_2 norm error gained by the EFG method is equal to 11.4 when reaching a mesh with $h = 1/16$. It may seem

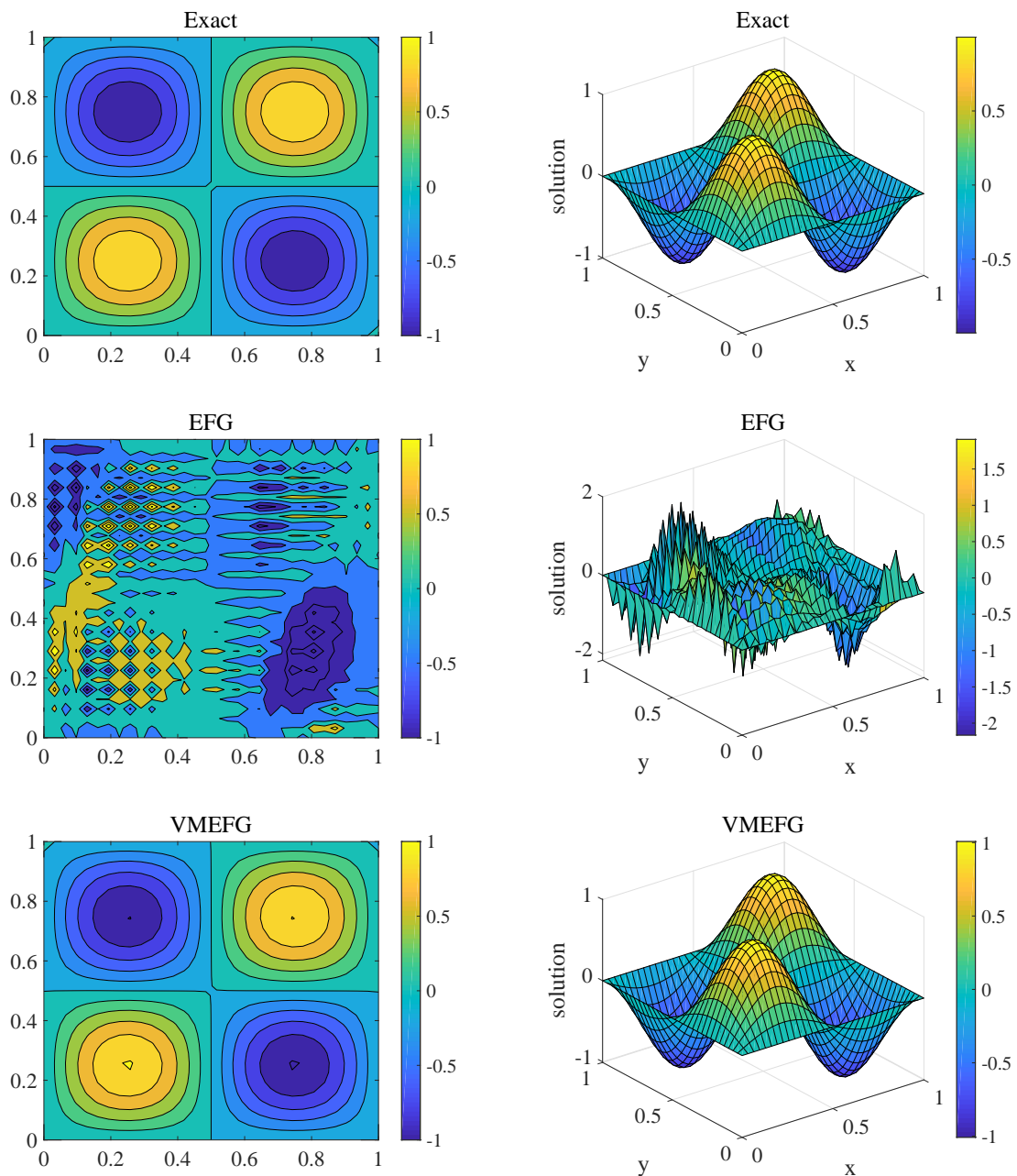


Fig. 8: The contour and elevation plots of solutions for Example 2 with 32^3 nodes in plane $z = 0.25$ (a) exact solution (first row); (b) EFG solution (second row); (c) VMEFG solution (third row).

too high. Meanwhile, the error computed by the VMEFG method is only equal to 0.0114. It can be calculated from the data given in Table III, the convergence rate of the VMEFG method approximates to 2. Hence, it is evident that the VMEFG method is extremely stable while solving this strong convection-dominated problem.

Fig.7 presents the numerical solutions and absolute errors resulting from the EFG and VMEFG methods with 32^3 nodes on the domain when $k = 10^{-6}$. It can be observed that the computed solutions of the EFG method are inaccurate enough, while the VMEFG method gains adequately accurate solutions. Fig.8 plots the exact and numerical results corresponding to the two methods in the xy plane with $z = 0.25$ when $k = 10^{-6}$. From Fig.8(b), it can be found that there are sharp non-physical oscillations that appear in the EFG solution. Nevertheless, Fig.8(c) is basically indistinguishable from the exact plots, showing

that the VMEFG solution is smooth without oscillations. Thus, the VMEFG method entirely prevents the oscillation problem in the EFG method. Moreover, the VMEFG method is still capable of giving stabilized and satisfying numerical solutions in this problem though the convection is strongly dominant.

Example3. This example considers the following differential equation in the absence of source term with small diffusion velocity and can find be in reference [36]

$$\begin{aligned}
 & -kU_{xx} - kU_{yy} - kU_{zz} - 2\tanh\left(\frac{x-0.5}{k}\right)U_x \\
 & - 2\tanh\left(\frac{y-0.5}{k}\right)U_y - 2\tanh\left(\frac{z-0.5}{k}\right)U_z = 0,
 \end{aligned}$$

whose exact solution is given by

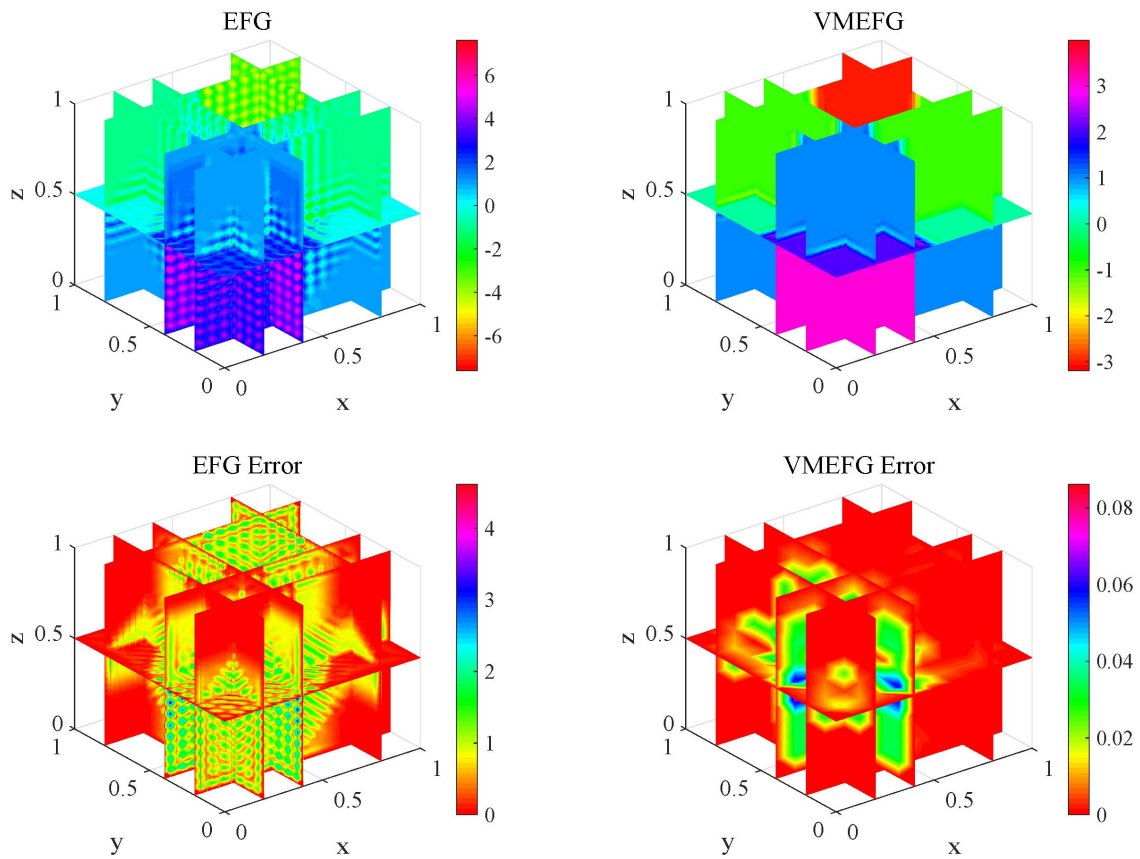


Fig. 9: The elevation plots of solutions for Example 3 with 32^3 nodes (a) EFG solution (top,left); (b) VMEFG solution (top,right); (c) EFG absolute error (bottom,left); (d) VMEFG absolute error (bottom,right).

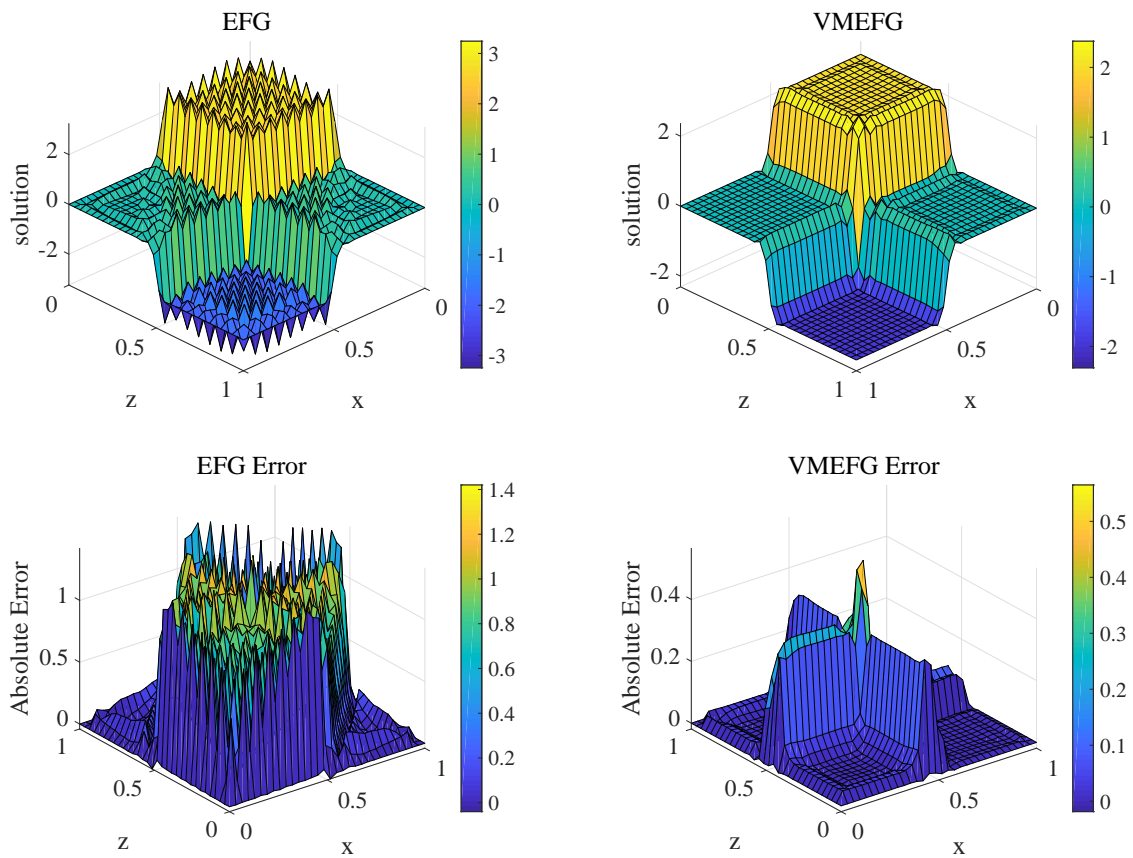


Fig. 10: The elevation plots of EFG and VMEFG solutions of Example 3 with 32^3 nodes in plane $y = 0.5$ (a) EFG solution (top,left); (b) VMEFG solution (top,right); (c) EFG absolute error (bottom,left); (d) VMEFG absolute error (bottom,right).

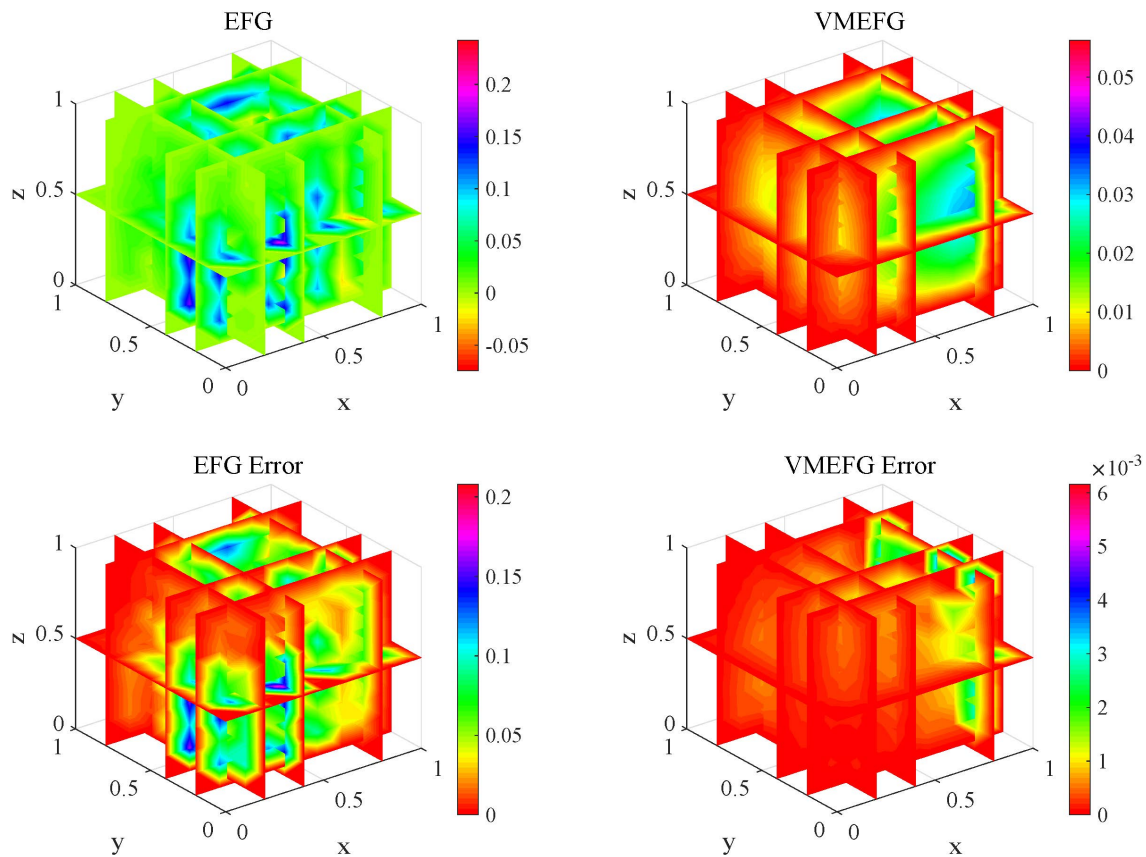


Fig. 11: The elevation plots of solutions for Example 4 with 8^3 nodes (a) EFG solution (top,left); (b) VMEFG solution (top,right); (c) EFG absolute error (bottom,left); (d) VMEFG absolute error (bottom,right).

$$U(x, y, z) = -\tanh\left(\frac{x-0.5}{k}\right) - \tanh\left(\frac{y-0.5}{k}\right) - \tanh\left(\frac{z-0.5}{k}\right).$$

The Dirichlet boundary conditions are determined from the exact solution. The calculations were carried out for the dominated case with $k = 10^{-3}$ using the EFG and the VMEFG method by calculating 32^3 nodes. Analogous to the previous examples, here we also present the plots of the numerical results and absolute errors in Fig.9. The results in Figs.9(a) and 9(b) show that the VMEFG solution is smooth while the EFG solution is not. From Figs.9(c) and 9(d), we also can find that the EFG method has large absolute errors, while the VMEFG method has relatively small errors in this case.

The numerical solutions and absolute error in the xz plane with $y = 0.5$ are depicted in Fig.10. As far as we are aware of the comparison between Figs.10(a) and 10(c), it can be clearly noted that only a few oscillations appear in the elevation plot for the VMEFG method. At the same time, the EFG solution has apparent spurious oscillations, which proves that the VMEFG significantly eliminates oscillations in the EFG method. As shown in Figs.10(d) and 10(e), it can be found that the error between the VMEFG solution and the exact solution is quite small, while the EFG solution has great errors. From what has been analyzed above, we can conclude that the VMEFG can vastly eliminate oscillations in the EFG method when the governing equation becomes convection-dominated, illustrating that the VMEFG method

is applicable to the convection-dominated problem.

Example4. This example considered is the convection-diffusion problem with a small constant diffusivity and the flow velocity being $c = [1, 1, 1]^T$. The exact solution can be referred to [37], given as below

$$U(x, y, z) = yz(1-y)(1-z) \left(x - \frac{e^{-(1-x)/v} - e^{-1/v}}{1 - e^{-1/v}} \right).$$

Taking the convection-dominated cases with $k = 10^{-3}$ into account, see Fig.11, the results are acquired by utilizing 8^3 nodes on the domain. Compared Fig.11(a) with Fig.11(b), the difference in the computational solutions between these two methods is quite big. But from Figs.11(c) and 11(d), it can be intuitively observed that the absolute error of the VMEFG method is much smaller than the EFG method. That is, the computed solutions of the EFG method are quite inaccurate compared to that of the VMEFG method, which owns very accurate solutions.

Fig.12 displays the numerical results in the xy plane with $z = 0.5$ computed by the EFG and VMEFG methods. From Fig.12(b), it can be easily found that nonphysical oscillations corrupt the numerical solution in the EFG method. Fig.12(c) demonstrates that the VMEFG solution agrees well with the exact solution. There are no oscillations appearing in the VMEFG method. Therefore, the VMEFG method can extremely avoid the oscillations that occur in the EFG method under this circumstance.

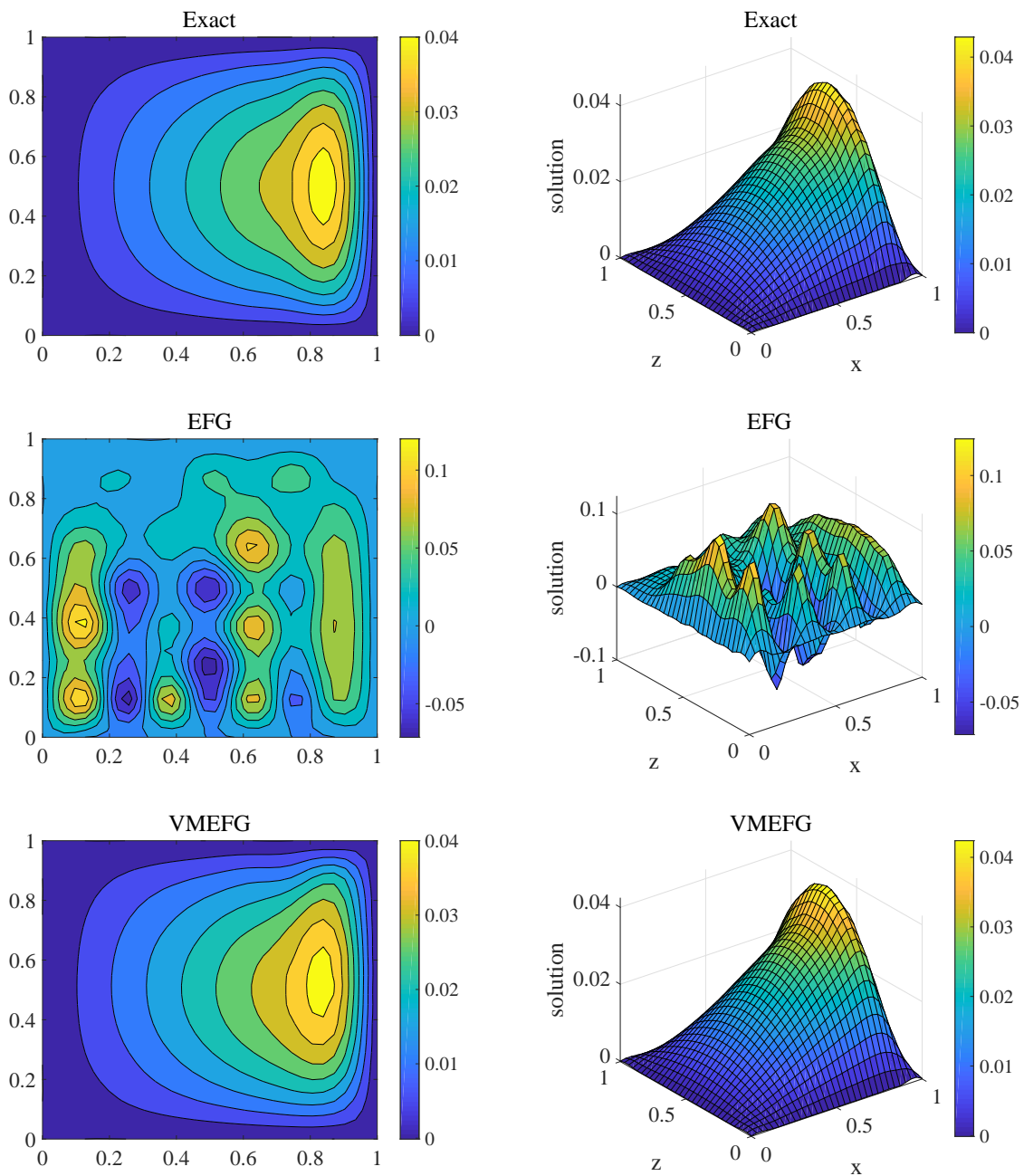


Fig. 12: The contour and elevation plots of solutions for Example 4 with 8^3 nodes in plane $z = 0.25$ (a) exact solution (first row); (b) EFG solution (second row); (c) VMEFG solution (third row).

V. CONCLUSIONS

In this paper, the VMEFG method is extended to address 3D steady convection-dominated problems. In this article, the bubble functions are used to determine the stability term naturally, which is closely associated with the stability and precision of the present method. The MLS approximation with an arbitrary convex polyhedral influence domain is employed to approximate the shape functions for the VMEFG method and let the nodal influence factor of the influence domain be equal to 1.01. This approach makes the MLS shape function interpolative, allowing the direct imposition of the boundary conditions to simplify the proposed method and improve the calculating efficiency. For illustrating the effectiveness of this method, four examples concerning the convection-diffusion equations have been solved. Numerical results indicate that the VMEFG method can virtually avoid

the nonphysical oscillations involved in the EFG method for dealing with the convection-dominated problem. Meanwhile, the VMEFG method possesses higher computational accuracy than the EFG method. Insufficiently, the VMEFG solution may exist a few oscillations in some highly convection-dominated problems.

It is famously known that the adaptive algorithm works well on refining nodes in the region where the solution drastically varies. So in further study, we can adopt the adaptive method to the VMEFG method for eliminating the above defect and more complicated problems. Besides, the adaptive VMEFG method can be applied for numerical experiments to further investigate the 3D convection-diffusion problems with time-dependent.

REFERENCES

- [1] A. Kaya, "Finite difference approximations of multidimensional unsteady convection-diffusion-reaction equations," *Journal of Computational Physics*, vol. 285, pp. 331-349, 2015.
- [2] R. Codina, "On stabilized finite element method for linear systems of convection-diffusion-reaction equations," *Computer Methods in Applied Mechanics and Engineering*, vol. 188, no. 1-3, pp. 61-82, 2000.
- [3] S. Phongthanapanich and P. Dechaumphai, "Finite volume method for convection-diffusion-reaction equation on triangular meshes," *Communications in Numerical Methods in Engineering*, vol. 26, no. 6, pp. 716-727, 2010.
- [4] G. R. Liu and Y. T. Gu, "An introduction to meshfree methods and their programming," Springer Science & Business Media, 2005.
- [5] S. Garg and M. Pant, "Meshfree Methods: A Comprehensive Review of Applications," *International Journal of Computational Methods*, vol. 15, no. 4, pp.1830001, 2018.
- [6] V. G. Patel and N. V. Rachhh, "Meshless method-Review on recent developments," *Materials today: proceedings*, vol. 26, no. 2, pp. 1598-1603, 2020.
- [7] W. Y. Tey, Y. Asako, K. C. Ng, and W. H. Lam, "A review on development and applications of element-free Galerkin methods in computational fluid dynamics," *International Journal for Computational Methods in Engineering Science and Mechanics*, vol. 21, no. 5, pp. 252-275, 2020.
- [8] P. Lancaster and K. Salkauskas, "Surfaces generated by moving least squares methods," *mathematics of computation*, vol. 37, no. 155, pp. 141-158, 1981.
- [9] Z. E. Majouti, R. E. Jid, and A. Hajjaj, "Solving Two-dimensional Linear and Nonlinear Mixed Integral Equations Using Moving Least Squares and Modified Moving Least Squares Methods," *IAENG International Journal of Applied Mathematics*, vol. 51, no. 1, pp. 57-65, 2021.
- [10] L. Z. Qian and H. P. Cai, "Two-grid method for characteristics finite volume element of nonlinear convection-dominated diffusion equations," *Engineering Letters*, vol. 24, no. 4, pp. 399-405, 2016.
- [11] X. H. Zhang and J. Ouyang, "Element Free Galerkin Method for Steady Convection Dominated Convection Diffusion Problem," *Chinese Quarterly of Mechanics*, vol. 27, no. 2, pp. 220-226, 2006.
- [12] X. H. Wu, Y. J. Dai, and W. Q. Tao, "MLPG/SUPG Method for Convection-Dominated Problems," *Numerical Heat Transfer, Part B: Fundamentals*, vol. 61, no. 1, pp. 36-51, 2012.
- [13] Z. J. Chen, Z. Y. Li, and W. Q. Tao, "A new stability parameter in streamline upwind meshless petrov-galerkin method for convection-diffusion problems at large pecllet number," *Numerical Heat Transfer, Part B: Fundamentals*, vol. 74, no. 5, pp. 746-764, 2018.
- [14] Y. J. Weng and Y. M. Cheng, "Analysis of variable coefficient advection-diffusion problems via complex variable reproducing kernel particle method," *Chinese Physics B*, vol. 22, no. 9, pp. 197-202, 2013.
- [15] E. C. Romão and L. F. Mendes de Moura, "Galerkin and Least Squares Methods to solve a 3D convection-diffusion-reaction equation with variable coefficients," *Numerical Heat Transfer, Part A: Applications: An International Journal of Computation and Methodology*, vol. 61, no. 9, pp. 669-698, 2012.
- [16] H. Cheng, M. Peng, and Y. M. Cheng, "A hybrid improved complex variable element-free Galerkin method for three-dimensional advection-diffusion problems," *Engineering Analysis with Boundary Elements*, vol. 97, pp. 39-54, 2018.
- [17] L. D. Ma, Z. J. Meng, J. F. Chai, and Y. M. Cheng, "Analyzing 3D advection-diffusion problems by using the dimension splitting element-free Galerkin method," *Engineering Analysis with Boundary Elements*, vol. 111, pp. 167-177, 2020.
- [18] J. Principe and R. Codina, "On the stabilization parameter in the subgrid scale approximation of scalar convection-diffusion-reaction equations on distorted meshes," *Computer Methods in Applied Mechanics & Engineering*, vol. 199, no. 21-22, pp. 1386-1402, 2010.
- [19] L. Zhang, J. Ouyang, X. X. Wang, and X. H. Zhang, "Variational multiscale element-free Galerkin method for 2D Burgers' equation," *Journal of Computational Physics*, vol. 229, no. 19, pp. 7147-7161, 2010.
- [20] L. Zhang, J. Ouyang, X. H. Zhang, and W. B. Zhang, "On a multiscale element-free Galerkin method for the Stokes problem," *Applied Mathematics and Computation*, vol. 203, no. 2, pp. 745-753, 2008.
- [21] L. Zhang, J. Ouyang, T. Jiang, and C. L. Ruan, "Variational multiscale element free Galerkin method for the water wave problems," *Journal of Computational Physics*, vol. 230, no. 12, pp. 5045-5060, 2011.
- [22] L. Zhang, J. Ouyang, and X. H. Zhang, "The variational multiscale element free Galerkin method for MHD flows at high Hartmann numbers," *Computer Physics Communications*, vol. 184, no. 4, pp. 1106-1118, 2013.
- [23] P. Zhang and X. H. Zhang, "Numerical modeling of stokes flow in a circular cavity by variational multiscale element free Galerkin method," *Mathematical Problems in Engineering*, vol. 2014, pp. 1-7, 2014.
- [24] J. H. Chen, X. H. Zhang, P. Zhang, and J. H. Deng, "Variational multiscale element free Galerkin method for natural convection with porous medium flow problems," *International Journal of Heat and Mass Transfer*, vol. 107, pp. 1014-1027, 2017.
- [25] T. Zhang and X. L. Li, "A variational multiscale interpolating element-free galerkin method for convection-diffusion and stokes problems," *Engineering Analysis with Boundary Elements*, vol. 82, pp. 185-193, 2017.
- [26] J. F. Wang and F. X. Sun, "A hybrid variational multiscale element-free Galerkin method for convection-diffusion problems," *International Journal of Applied Mechanics*, vol. 11, no. 7, pp. 1950063, 2017.
- [27] M. Dehghan and M. Abbaszadeh, "Variational multiscale element-free Galerkin method combined with the moving Kriging interpolation for solving some partial differential equations with discontinuous solutions," *Computational and Applied Mathematics*, vol. 37, no. 3, pp. 3869-3905, 2018.
- [28] S. Peddavarapu and S. Raghuraman, "Maximum entropy-based variational multiscale element-free Galerkin methods for scalar advection-diffusion problems," *Journal of Thermal Analysis and Calorimetry*, vol. 141, pp. 2527-2540, 2020.
- [29] T. Belytschko, Y. Y. Lu, and L. Gu, "Element-free Galerkin methods," *International Journal for Numerical Methods in Engineering*, vol. 37, no. 2, pp. 229-256, 1994.
- [30] V. P. Nguyen, T. Rabczuk, S. Bordas, and M. Duflot, "Meshless methods: a review and computer implementation aspects," *Mathematics and Computers in Simulation*, vol. 79, no. 3, pp. 763-813, 2008.
- [31] X. H. Zhang, P. Zhang, and L. Zhang, "An improved meshless method with almost interpolation property for isotropic heat conduction problems," *Engineering Analysis with Boundary Elements*, vol. 37, no. 5, pp. 850-859, 2013.
- [32] X. H. Zhang, J. Ouyang, and J. Y. Wang, "Stabilization meshless method for convection-dominated problems," *Applied Mathematics and Mechanics*, vol. 29, no. 8, pp. 1067-1075, 2008.
- [33] A. Masud and R. A. Khurram, "A multiscale/stabilized finite element method for the advection-diffusion equation," *Computer Methods in Applied Mechanics and Engineering*, vol. 193, no. 21-22, pp. 1997-2018, 2004.
- [34] X. H. Zhang and H. Xiang, "Variational multiscale element free Galerkin method for convection-diffusion-reaction equation with small diffusion," *Engineering Analysis with Boundary Elements*, vol. 46, pp. 85-92, 2014.
- [35] G. R. Barrenea, A. H. Poza, and H. Yorston, "A stabilised finite element method for the convection-diffusion-reaction equation in mixed form," *Computer Methods in Applied Mechanics and Engineering*, vol. 339, pp. 389-415, 2018.
- [36] N. Mohamed, S. A. Seddek, and L. F. Mohamed, "Exponential higher-order compact scheme for 3D steady convection-diffusion problem," *Applied Mathematics and Computation*, vol. 232, pp. 1046-1061, 2014.
- [37] M. Ainsworth, A. Allendes, G. R. Barrenea, and R. Rankin, "Fully computable a posteriori error bounds for stabilised FEM approximations of convection-reaction-diffusion problems in three dimensions," *International Journal for Numerical Methods in Fluids*, vol. 73, no. 9, pp. 765-790, 2013.